Journal of Applied Fluid Mechanics, Vol. 17, No. 12, pp. 2734-2744 2024.
Available online at www.jafmonline.net, ISSN 1735-3572, EISSN 1735-3645.
https://doi.org/10.47176/jafm.17.12.2707

Experimental Study on Evolution of Cavitation Flow Structure in Hump Region of Waterjet Pump

Y. Long[1†], Z. Zhou[1], J. Zhong[1] and H. Han[2]

[1] *National Research Center of Pumps, Jiangsu University, Zhenjiang, Jiangsu, 212013, China*
[2] *Wuhan Second Ship Design and Research Institute, Wuhan, Hubei, 430064, China*

†*Corresponding Author Email: longyun@ujs.edu.cn*

ABSTRACT

The waterjet propulsor is a new type of marine propulsion system, which offers the advantages of high speed, good maneuverability, and low vibration and noise. As the core component of the waterjet propulsor, the primary role of the waterjet pump is to provide sufficient thrust for the vessel. However, the waterjet pump is prone to be troubled by the hump phenomenon. As the pump operates in the hump region, it may encounter issues such as flow interference and exacerbated vibration and noise, which are closely related to cavitation phenomenon in the pump. To analyze the evolution of cavitation flow structure in the waterjet pump when operating in the hump region, this study utilized high-speed photography to obtain the cavitation flow structure at different cavitation development stages under the hump peak condition. The cavitation stages involved include the cavitation inception stage, cavitation development transition stage, first critical cavitation stage, critical cavitation stage, and breakdown cavitation stage. During different cavitation development stages under the hump peak condition, the blade tip region exhibits distinct cloud cavitation induced by the tip leakage vortex (TLV). As the *NPSH* decreases, the frequency of cloud cavitation shedding increases, the scale of the cavitation cloud at the leading edge of the blade decreases, and the scale of the cavitation cloud accumulated at the rear of the flow passage increases. This study on the cavitation flow of the waterjet pump is significant as it contributes to enhancing the anti-cavitation performance and reducing vibration and noise. It provides scientific guidance and engineering practice for improving the safety and stability of waterjet pumps during operation.

Article History

Received March 7, 2024
Revised May 27, 2024
Accepted June 30, 2024
Available online October 2, 2024

Keywords:

Waterjet pump
Hump region
Cavitation
Vortex structure
High-speed photography

1. INTRODUCTION

The waterjet pump is the core component of the waterjet propulsor, undertaking the important function of converting mechanical energy into fluid kinetic energy. Limited by the installation and layout conditions of the carrier, axial flow pumps or mixed flow pumps with diffusers are the preferred choice for the waterjet pumps. However, axial flow pumps and mixed flow pumps with high specific speeds are prone to exhibiting a hump or even double humps at the head-flow curve. The unusual inflection point at the pump head-flow curve, referred to as the hump phenomenon, is illustrated in Fig. 1. In this paper, the operating condition corresponding to the minimum point in the hump region of the head-flow curve is called hump valley condition, and the operating condition corresponding to the maximum point is called hump peak condition. In order to adapt to different speeds

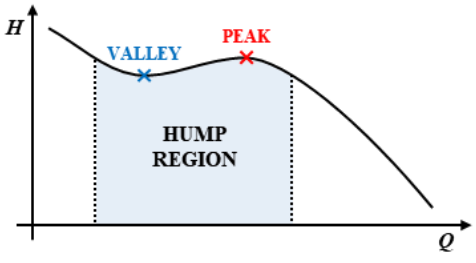

Fig. 1 Schematic diagram of hump phenomenon

of vessels, the waterjet pump needs to adjust the flow rate and rotation speed, which often results in its long-term operation under off-design flow conditions. While operating in the hump region, both the pump and even the entire system may experience problems such as flow

disturbance, increased vibration and abnormal noise (Huang et al., 2022; Wang & Ding, 2022; Yang et al., 2023).

The academic community generally believes that the fundamental reason for the formation of hump region is the alteration in the flow pattern of the pump. Some scholars (Iino & Tanaka, 2004; Li et al., 2016; Ran & Luo, 2018; Ran et al., 2020) suggested a correlation between the occurrence of the hump and the phenomenon of flow separation in the impeller and diffuser. Additionally, some scholars believe that flow separation in the diffuser plays a more important role in the formation of hump (Cao et al., 1999; Guedes et al., 2002; Guleren & Pinarbasi, 2004; Shibata et al., 2016). More directly, there are two viewpoints that can explain the reason for the hump at the energy characteristic curve. One interpretation posits that the alteration in flow pattern contributes to the non-monotonic variation in hydraulic loss, leading to the formation of the hump. The other interpretation posits that the alteration in flow pattern contributes to the variation in power capability of the impeller, leading to the formation of the hump.

According to Xiao et al. (2016), the occurrence of the hump is associated with significant hydraulic loss caused by secondary flow, backflow, and vortex in the draft tube, runner, and guide vanes. Li et al. (2017) argue that the hump characteristics are the result of the combined effect of the Euler momentum and energy loss. Through the analysis of entropy generation, it was found that the hump hysteresis characteristics are attributed to the backflow at the impeller inlet, as well as the vortex structure in the stay vanes and guide vanes. According to Ye et al. (2020, 2021), the significant rise of energy loss in the impeller is the primary reason for the occurrence of hump characteristics. The flow separation is the main source of energy loss, which alters the distribution of blade loading, leading to a sudden drop in head. Liu et al. (2021) conducted a study on a double-suction centrifugal pump and found that the primary cause of hump is the reduction in power capability of the impeller due to diffuser stall. Additionally, the increase in asymmetrical flow and turbulence intensity in the volute leads to an increase in hydraulic loss. Zhao et al. (2022) found that the emergence of the hump arises from the interaction between the horn-like vortex and the leading edge backflow in the impeller. The leading edge backflow decreases the power capability of the impeller, and the horn-like vortex enhances the power capability of the impeller.

Cavitation significantly affects both the thrust and propulsion efficiency of waterjet pumps. The cavitation in the waterjet pump not only reduces the propulsion efficiency and axial thrust of the propulsor, but also increases the vibration and noise during the operation, and may lead to erosion damage on the surface of hydraulic components. This affects the operational stability of the waterjet propulsor and seriously threatens the navigation safety of waterjet propulsion vessels.

Through cavitation visualization experiment combined with numerical simulation, Long et al. (2020, 2021a, b, 2023) captured the evolution of cavitation flow structure in a waterjet pump during different cavitation development stages, and analyzed the impact of different cavitation structures on the performance of the waterjet pump. Huang et al. (2021) conducted a study on the unsteady cavitation flow in a waterjet pump under the non-uniform inflow condition, and obtained the interaction mechanism between cavitation and vortices, as well as analyzed the pressure fluctuation characteristics caused by cavitation. Zhao et al. (2021) studied the dynamic characteristics of blade cavitation under the disturbance from inlet guide vane wakes in a waterjet pump. It is pointed out that the influence of inflow distortion on blade cavitation cannot be ignored, resulting in severe cavitation oscillation and subsequently impeller vibration. Arabnejad et al. (2021, 2022) utilized their developed cavitation erosion numerical assessment method to assess the potential for erosion of a waterjet pump. Comparison with experimental results demonstrated that this numerical method is able to identify regions prone to erosion damage and capture variations in erosion risk under different operating conditions.

Numerous scholars have confirmed the existence of a certain relationship between hump characteristics and cavitation. Ješe et al. (2015) found that cavitation at the impeller inlet reduces the hump amplitude and increases the energy loss in the impeller and distributor. Liu et al. (2015) pointed out that the hump characteristic is sensitive to cavitation number. As the cavitation number decreases, the hump of the head-flow curve gradually decreases until it disappears. Li et al. (2015, 2019, 2021, 2022) conducted a study on the cavitation phenomenon of a pump-turbine in the hump region. They found that the formation of the hump is attributed to the cavitation on the suction side of the blade close to the leading edge. The cavitation causes a reduction in the Euler head, a rise in energy loss, and subsequently a reduction in head. Additionally, they revealed the mechanism through which cavitation affects pressure fluctuations in the hump region. The cavitation significantly affects the low frequency pressure fluctuation, leading to variations in the hump characteristic.

To conclude, numerous researchers have extensively studied different types of pumps for the hump at the head-flow curve. There remains a lack of agreement regarding the cause of the hump, and comparatively few studies have been conducted on the cavitation flow in the hump region. Studying cavitation phenomenon in the hump region of waterjet pumps contributes to enhancing the anti-cavitation performance of waterjet propulsors, thereby improving the operational safety and stability. In this paper, a cavitation visualization experiment was conducted, capturing the flow structure in a waterjet pump. The cavitation flow structures and their evolution process during various cavitation development stages were analyzed under the hump peak condition.

2. CAVITATION EXPERIMENT

2.1 Waterjet Pump Model

For the experiment, the mixed flow waterjet pump is chosen as the research object. Table 1 shows the main

(a) Impeller (b) Diffuser (c) Impeller chamber

Fig. 2 Real hydraulic components of waterjet pump

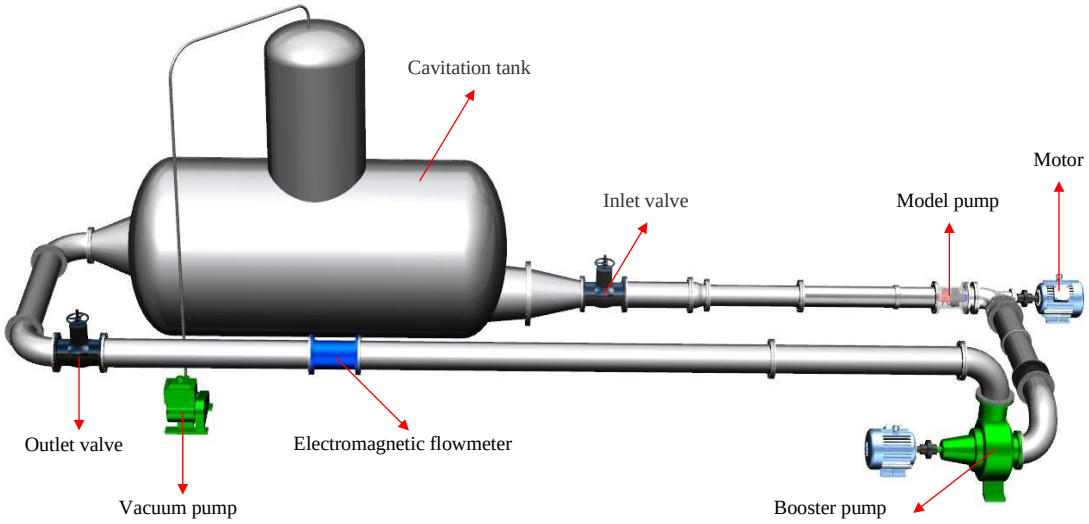

Fig. 3 Schematic diagram of closed-type test bench

Table 1 Basic parameters of test pump

Design Parameters	Design Value
Flow rate Q (m^3/s)	0.46
Head H (m)	11
Rotation speed n (r/min)	1200
Impeller inlet diameter D_j (mm)	250
Impeller blade number Z_1	6
Diffuser blade number Z_2	11
Tip clearance δ (mm)	1

design parameters of the model pump. Figure 2 shows the main hydraulic components.

2.2 Pump Comprehensive Performance Test Bench

The cavitation experiment is conducted on a closed-circulation experimental system of axial flow pumps and mixed flow pumps. Figure 3 is the schematic diagram of the closed-type test bench, including the motor, model pump, inlet valve, outlet valve, electromagnetic flowmeter, cavitation tank, vacuum pump and booster pump. Regarding the test system, the measurement accuracy of flow, pressure and torque is 0.2 %. The adjustable-speed motor is set to the test speed, and the flow rate is regulated to the test condition. After the pump stabilizes in operation, the vacuum pump is started to evacuate the cavitation tank, gradually reducing the pressure at the pump inlet and inducing cavitation in the pump. The process of the decline of the head curve under different inlet pressures is recorded. The pump inlet pressures corresponding to the cavitation inception stage, cavitation development transition stage, first critical cavitation stage, critical cavitation stage, and breakdown cavitation stage are determined based on the head curve. By controlling the vacuum pump and adjusting the valve, the inlet pressure is adjusted to the inlet pressure corresponding to the different cavitation stages of the current flow condition point. Utilizing a high-speed camera, the cavitation flow structures under different cavitation stages are captured.

2.3 High-Speed Photography Collection System

The iX Cameras i-SPEED 3 high-speed camera is used, with a maximum resolution of 1280×1024 and a maximum frame rate of 150000 fps. When capturing at the maximum resolution, the maximum frame rate is 2000 fps, and when capturing at the maximum frame rate, the resolution is 60×44. The position and evolution process of cavitation in the waterjet pump are photographed by this camera. To capture the cavitation flow structure in the impeller of the pump, the impeller chamber is made of plexiglass. To minimize the image distortion resulting from light refraction, the plexiglass impeller chamber features a square outside and a circular inside. Before shooting, adjust the center of the camera lens to the same height as the horizontal meridional plane of the impeller,

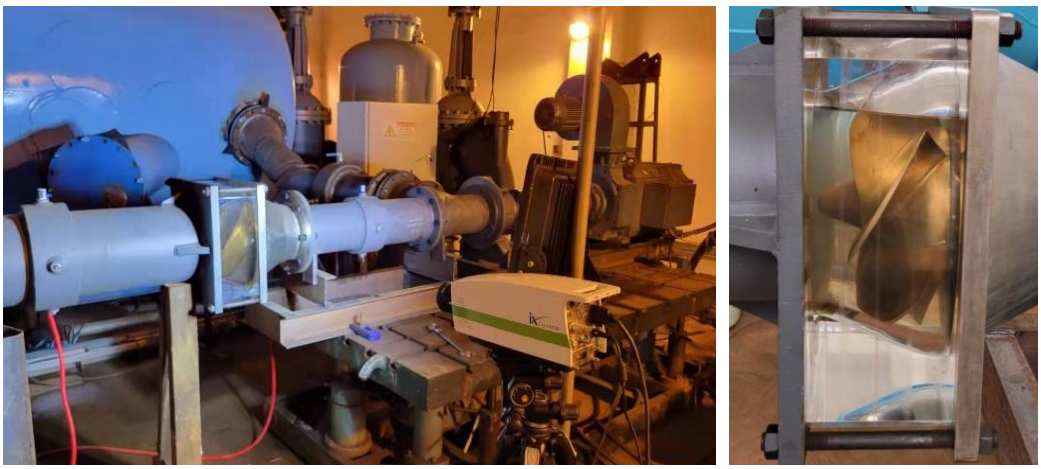

Fig. 4 High-speed photography visualization experiment system

and align the camera axis perpendicular to the vertical meridional plane of the impeller. The camera is set to shoot from the side of the impeller. Figure 4 shows the layout of the cavitation visualization test bench. The impeller can be clearly seen through the transparent impeller chamber with water, which indicates that the design scheme is reasonable.

The intensity of the light source required for the high-speed camera depends on the selected frame rate. When the intensity of natural light is not sufficient to meet the requirements of the frame rate, external lighting equipment should be used to provide additional illumination. Additionally, the image clarity is closely related to the selection of the frame rate for the camera. Selecting a frame rate that is too low results in increased exposure time, causing image blur and loss of flow details in the pump. Selecting a frame rate that is too high leads to a shortened duration of captured images, potentially resulting in incomplete depiction of evolution process and inability to meet subsequent analysis requirements. Therefore, selecting the appropriate shooting frame rate is crucial for achieving optimal image quality. Based on the lighting condition of the test site and the necessity of image clarity, along with the function parameters of the camera, the shooting frame rate in this experiment is ultimately set at 2000 fps, with a corresponding image resolution of 1280×1024.

In order to obtain the cavitation flow in the model pump, if the impeller rotation speed is n and the frame rate is f, the rotation angle α of the impeller captured in each frame is:

$$\alpha=\frac{n\times 360/60}{f} \tag{1}$$

Where, α is the rotation angle of the impeller, °, and n is the rotation speed of the impeller, r/min. In this experiment, the shooting frame rate is 2000 fps, which means that an image is captured every 3.6° of impeller rotation.

2.4 Results of Cavitation Experiment

In order to make the experimental results more universally applicable, the data of flow rate (Q), head (H), and impeller torque (T) are dimensionless transformed according to the standards of the International Electrotechnical Commission (IEC), utilizing the expressions below:

$$Q_{\mathrm{nD}}=\frac{Q}{nD^3} \tag{2}$$

$$E_{\mathrm{nD}}=\frac{gH}{n^2D^2} \tag{3}$$

$$T_{\mathrm{nD}}=\frac{T}{\rho n^2D^5} \tag{4}$$

Where, Q_{nD}, E_{nD}, and T_{nD} respectively represent the flow coefficient, energy coefficient, and torque coefficient, which are dimensionless numbers. Q is flow rate, m^3/s; n is rotation speed, r/min; D is the nominal diameter of impeller, m; g is the acceleration of gravity, m/s^2; H is head, m; T is torque, N·m; ρ is density, kg/m^3.

Figure 5 shows the hydraulic performance curves of the waterjet pump. Obviously, the energy characteristic curve exhibits the form of double humps. Since the second hump region is closer to the design condition of the pump, this paper only focuses on the second cavitation phenomenon in the hump region. Due to the limited number of flow rate points selected for cavitation performance testing, the positions of the valley and peak can only be roughly determined. Based on the variation of the energy characteristic curve, the flow condition of Q_{nD}=0.014 is selected as the near-valley condition, and the flow condition of Q_{nD}=0.016 is selected as the near-peak condition. This paper only analyzes the cavitation flow structure and its evolution process under the near-peak condition.

In the cavitation performance experiment, Net Positive Suction Head (*NPSH*) is used as a crucial parameter to assess the likelihood of cavitation occurring in a pump. *NPSH* indicates the amount of head that exceeds the vapor pressure of the fluid at the inlet of a pump. The expression for *NPSH* is as follows:

$$NPSH=\frac{p_{\mathrm{s}}}{\rho g}+\frac{v_{\mathrm{s}}^2}{2g}-\frac{p_v}{\rho g} \tag{5}$$

Where, p_{s} is the pressure at the pump inlet, v_{s} is the velocity at the pump inlet, and p_v is the saturated vapor pressure of the liquid. During the experiment, the *NPSH* is gradually reduced until the ratio of the decrease in pump head to the pump head at a constant flow rate reaches 3%. The *NPSH* value at this point is defined as $NPSH_{\mathrm{c}}$.

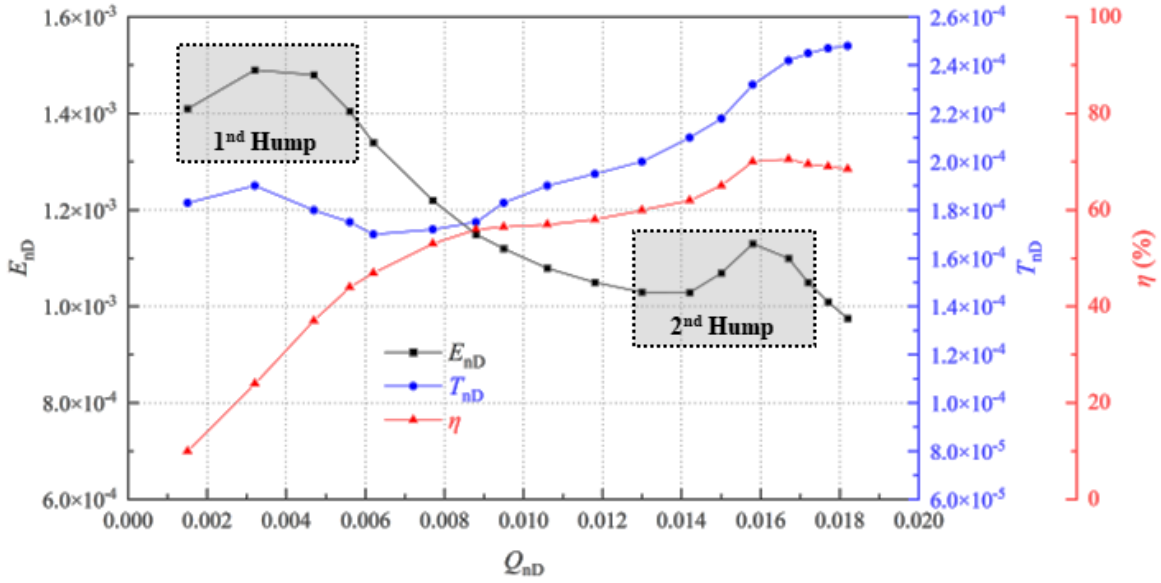

Fig. 5 Hydraulic performance curves of model pump

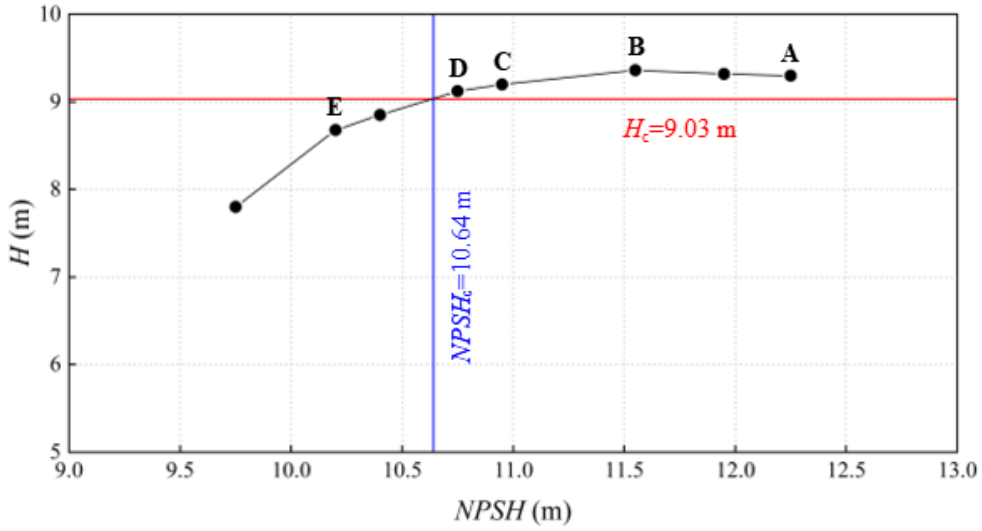

Fig. 6 Cavitation performance curve under near-peak condition

Figure 6 shows the cavitation performance curve of the model pump under the near-peak condition. Points A-D in the figure represent the condition points corresponding to different cavitation development stages at the cavitation performance curve. Although the head of the test pump remains relatively constant at the initial condition of the cavitation experiment, significant cavitation already exists in the pump. Therefore, this condition is defined as the cavitation inception stage, with Point A selected as its representative. As the *NPSH* decreases, the head starts to decrease slightly, and then the decrease becomes more pronounced. This condition corresponds to Point C on the cavitation performance curve, which is referred to as the first critical cavitation stage. To more comprehensively demonstrate the evolution of cavitation flow structure, Point B, located between Point A and Point C, is defined as the cavitation development transition stage. When the head decreases by 3%, it approximately corresponds to Point D on the cavitation performance curve, which is defined as the critical cavitation stage. As the *NPSH* continues to decrease, the decrease in head of the test pump becomes even greater. At this time, Point E is selected and defined as the breakdown cavitation stage. As shown in Fig. 7, based on the various condition points selected from the cavitation performance curve, the evolution process of cavitation flow structure in the pump during different cavitation development stages is presented.

3. Evolution of Cavitation Flow Structure

To fully reveal the space-time evolution process of cavitation in the hump region, the cavitation flow structures during different cavitation development stages under the near-peak condition are analyzed.

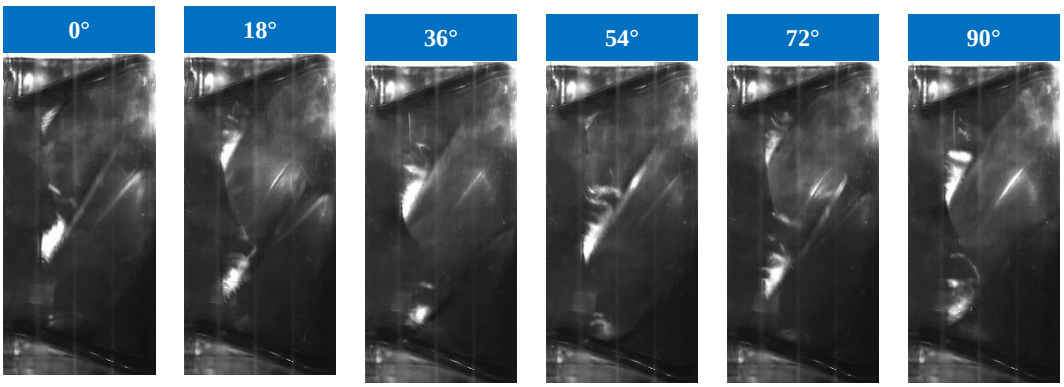

(a) Cavitation inception stage

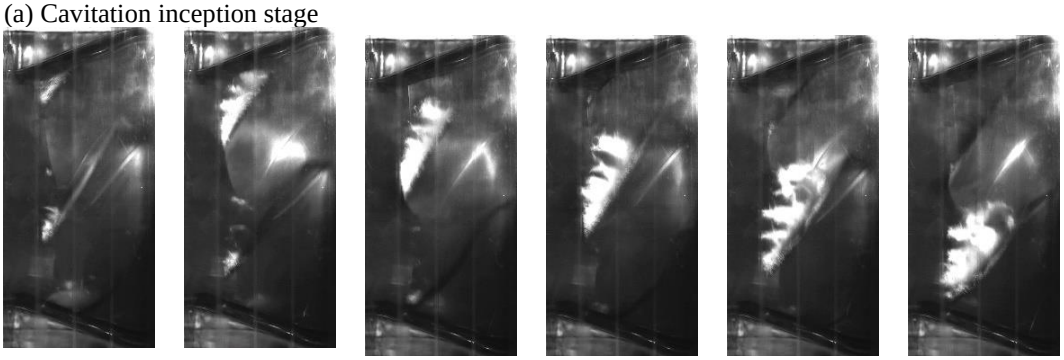

(b) Cavitation development transition stage

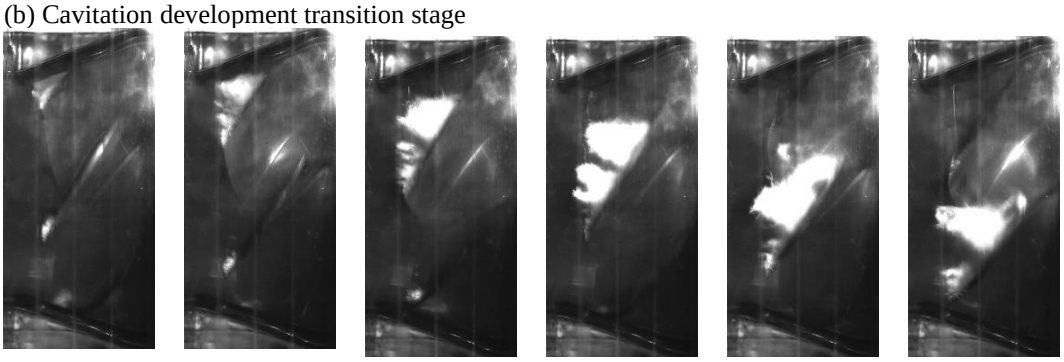

(c) First critical cavitation stage

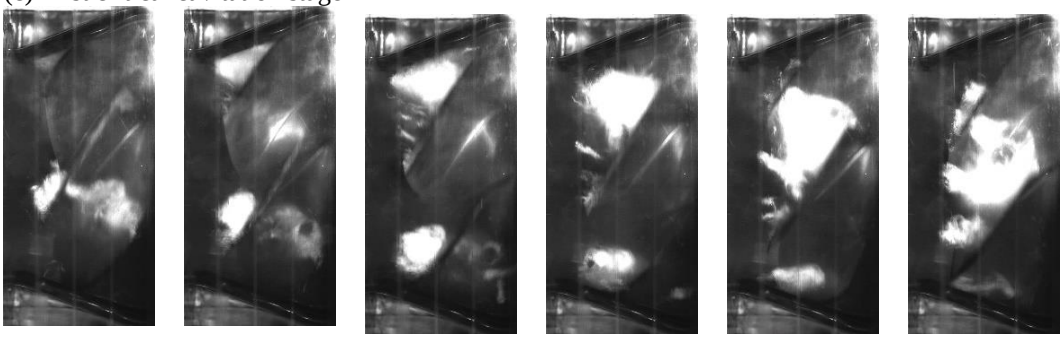

(d) Critical cavitation stage

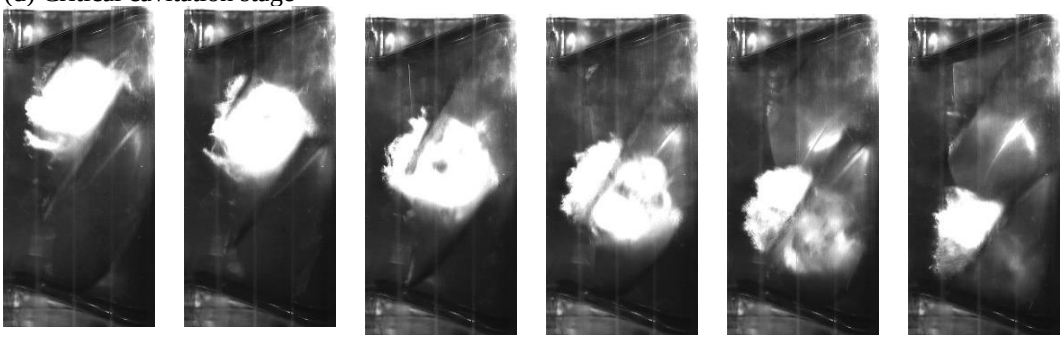

(e) Breakdown cavitation stage

Fig. 7 Evolution of cavitation flow structure in pump under near-peak condition

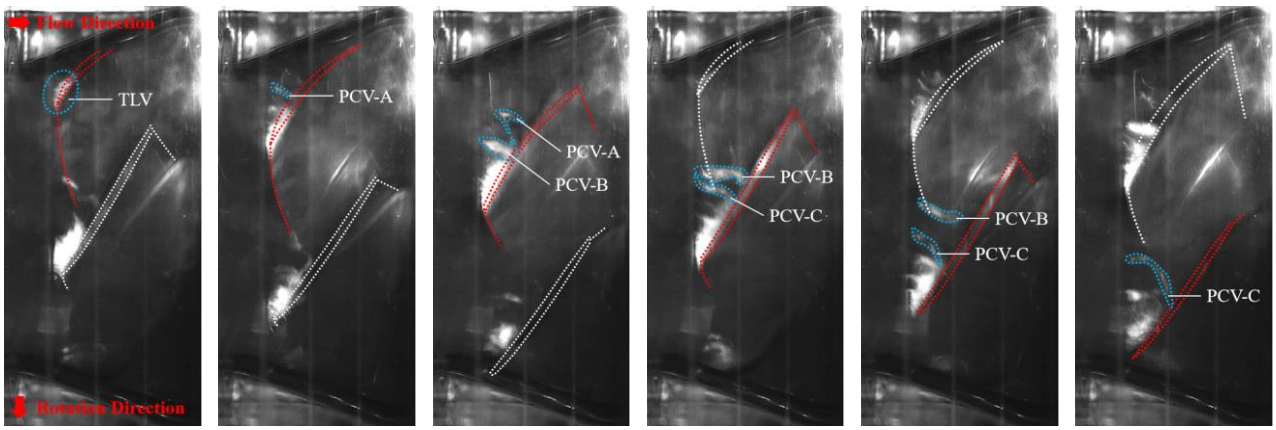

Fig. 8 Cavitation flow structure of cavitation inception stage

3.1 Cavitation Inception Stage

Figure 8 illustrates the evolution process of cavitation flow structure in the waterjet pump during the cavitation inception stage (Point A at the cavitation performance curve). From the figure, it can be observed that the cavitation flow structures in the adjacent flow passages are similar. There is obvious cloud cavitation induced by the tip leakage vortex (TLV) in the blade tip region. In the middle of the blade, periodic shedding of the cavitation clouds occurs. The shed cavities move in the direction of the main flow under the influence of the main flow. As the impeller rotates through 18°, the vortex filament shedding from the main cavitation region can be observed. The vortex filament, which is approximately perpendicular to the blade, is known as the perpendicular cavitation vortex (PCV), denoted as PCV-A. The shed PCV-A gradually moves towards the middle of the flow passage. As the impeller rotates through 36°, PCV-A completely sheds from the main cavitation region, and a new shed cavitation cloud, PCV-B, emerges upstream. As the impeller rotates through 54°, PCV-A rapidly collapses in the flow passage. Simultaneously, with the development of PCV-B, the emergence of PCV-C can be observed. As the impeller continues to rotate, this periodic shedding will persist. As the impeller rotates through 90°, PCV-B has already collapsed in the flow passage, and PCV-C has completely shed from the main cavitation region.

3.2 Cavitation Development Transition Stage

Figure 9 illustrates the evolution process of cavitation flow structure during the cavitation development transition stage (Point B at the cavitation performance curve). Compared to the cavitation inception stage, during this stage, the cavitation region extends towards the direction of the main flow, the frequency of cloud cavitation shedding is higher, the scale of the shed cavitation clouds is larger, and the cavitation flow structures in adjacent flow passages are not similar. As the impeller rotates through 72°, the cavitation region is even divided into 4 cavitation clouds with distinct boundaries. As the impeller rotates through 90°, the shed cavitation clouds are unable to maintain their boundaries and gradually collapse in the flow passage. Simultaneously, it can be observed that the wake at the end of the cavitation region is perpendicular to the blade. During this stage, the pressure side of the adjacent blade shows limited impact from the TLV, with no cavities appearing. Consequently, there is no significant drop in the cavitation performance curve.

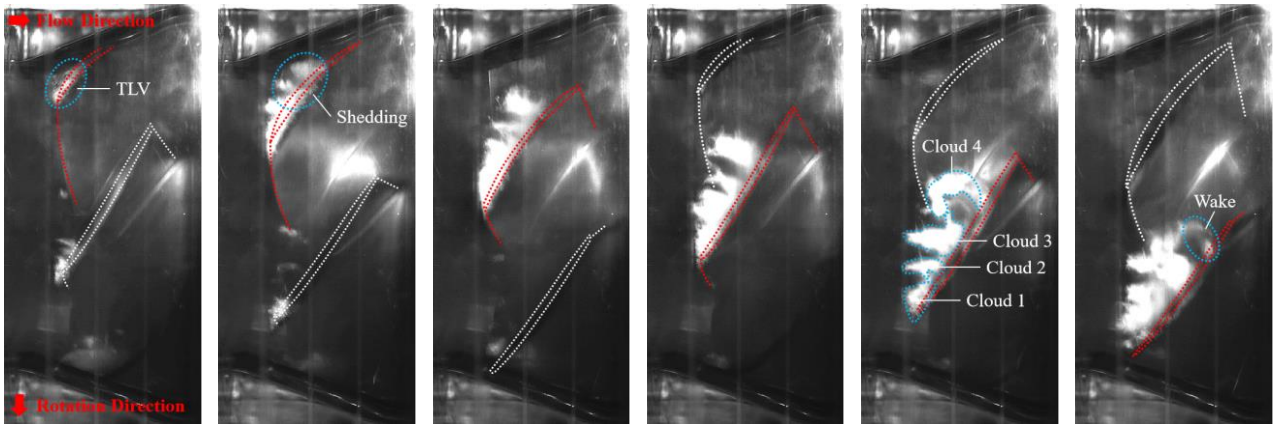

Fig. 9 Cavitation flow structure of cavitation development transition stage

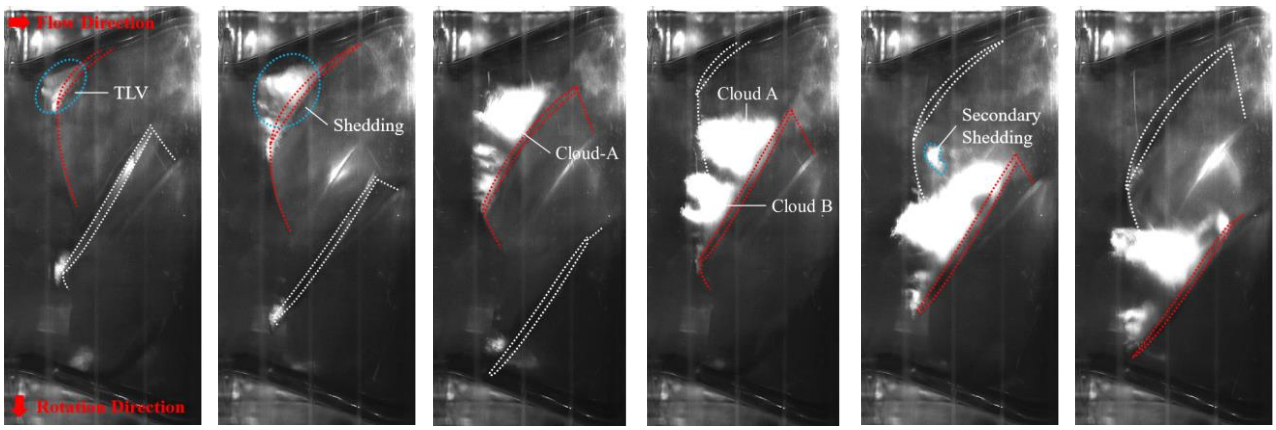

Fig. 10 Cavitation flow structure of first critical cavitation stage

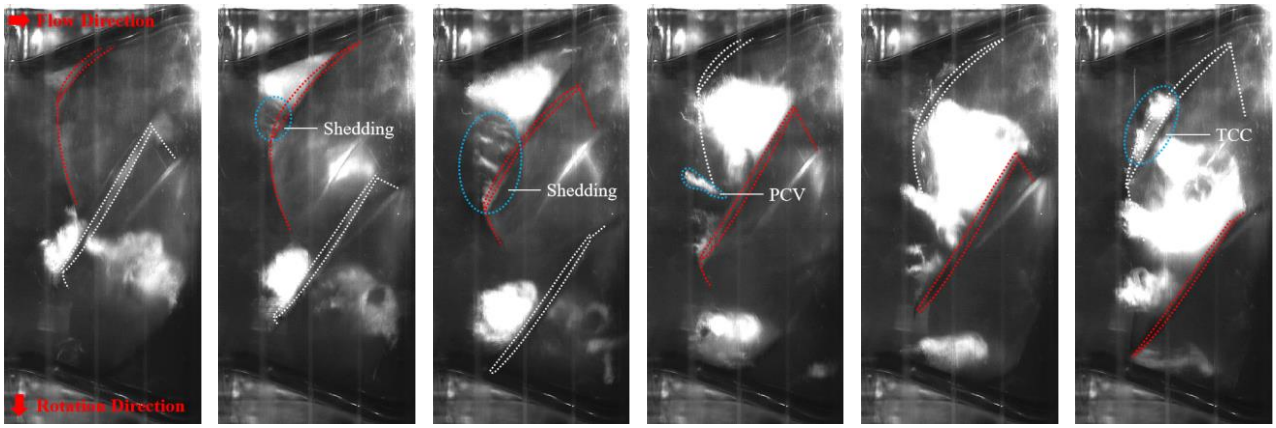

Fig. 11 Cavitation flow structure of critical cavitation stage

3.3 First Critical Cavitation Stage

Figure 10 illustrates the evolution process of cavitation flow structure during the first critical cavitation stage (Point C at the cavitation performance curve). During this stage, the scale of the cavitation cloud at the leading edge of the blade has noticeably diminished. Generally, the cavities shed from the main cavitation region will rapidly collapse due to the lack of energy replenishment. However, the shed cavities gradually accumulate, forming a significant cavitation cloud at the middle of the blade, designated as Cloud-A (with the impeller at a 36° rotation angle). As the impeller rotates through 54°, the cloud cavitation at the leading edge of the blade almost completely sheds and forms another cavitation cloud, Cloud-B, with a distinct boundary downstream. As the impeller continues to rotate, these two cavitation clouds interfere with each other and gradually collapse in the middle of the flow passage. As the impeller rotates through 72°, a small-scale cavitation cloud can be observed undergoing secondary shedding and moving towards the adjacent blade. Meanwhile, cavities begin to reaccumulate at the leading edge of the blade. As the impeller rotates through 90°, a cavitation cloud of a certain scale re-forms at the leading edge of the blade.

3.4 Critical Cavitation Stage

Figure 11 illustrates the evolution process of cavitation flow structure during the critical cavitation stage (Point D at the cavitation performance curve). As can be observed from the figure, the cavities caused by TLV rapidly shed from the leading edge of the blade and accumulate in the middle to rear section of the flow passage, forming a large-scale cavitation cloud. As the impeller rotates, the cavitation cloud rapidly moves towards the adjacent blade, blocking the entire flow passage. As the impeller rotates through 72°, flow separation occurs on the pressure side of the blade due to the influence of the shed cavitation cloud. As the impeller rotates through 90°, the shed cavities move towards the tip clearance of the adjacent blade, causing the tip clearance cavitation (TCC). During this stage, cavitation in the pump has become very severe, significantly affecting the performance of the pump and causing a reduction in the head by approximately 3%.

3.5 Breakdown Cavitation Stage

Figure 12 illustrates the evolution process of cavitation flow structure during the breakdown cavitation

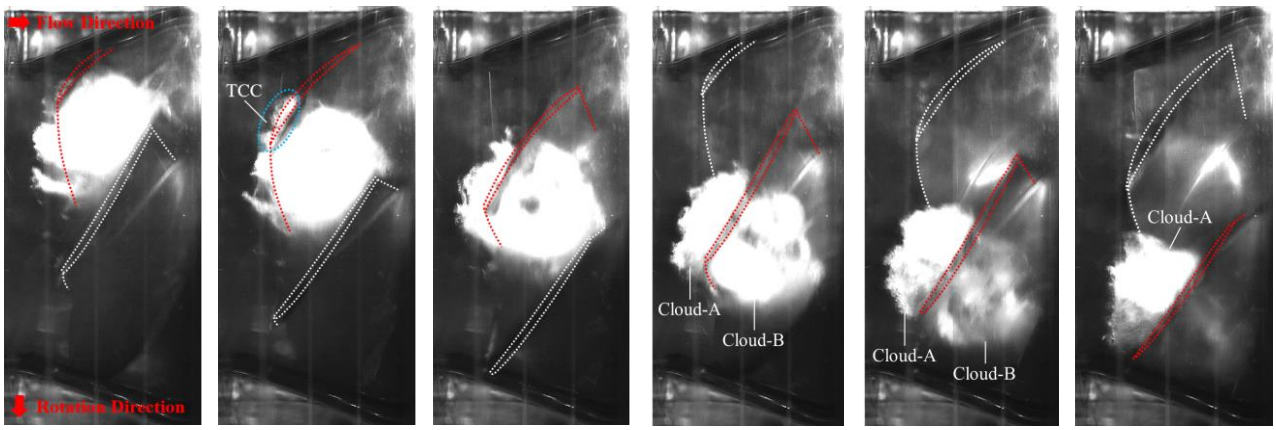

Fig. 12 Cavitation flow structure of breakdown cavitation stage

stage (Point E at the cavitation performance curve). As shown in the figure, severe cavitation occurs in the pump,with the cavitation cloud completely blocking the flow passage and covering the leading edge of the blade. As the impeller rotates, the blade gradually cuts through the cavitation cloud. As the impeller rotates through 54°, the blade completely splits the cavitation cloud into two parts. The cavitation cloud Cloud-A on the pressure side directly collapses on the blade surface, causing blade erosion and inducing vibration and noise. The cavitation cloud Cloud-B on the suction side moves towards the pressure side of the adjacent blade, thereby inducing cavitation on the adjacent blade. During this stage, the large-scale cavitation cloud has a serious impact on the flow in the pump, causing secondary flows in the flow passage and flow separation on the blade surface, leading to a sharp decline in pump performance.

4. CONCLUSION

Through cavitation visualization experiment, this study analyzes the cavitation flow structures during different cavitation development stages under the hump peak condition of a waterjet pump, and explores the evolution law of cavitation and its impact on pump performance. The primary contributions and findings of this study are as follows:

(1) A comprehensive performance experiment platform for waterjet pumps was established, obtaining the hydraulic performance curve and the cavitation performance curves under the hump peak condition (Q_{nD}=0.016). Based on variations in head and cavitation flow structure during the cavitation experiment, different cavitation development stages of the waterjet pump were defined, including the cavitation inception stage, cavitation development transition stage, first critical cavitation stage, critical cavitation stage, and breakdown cavitation stage.

(2) During different cavitation development stages under the hump peak condition, there exists distinct cloud cavitation in the blade tip region induced by the tip leakage vortex (TLV). The cloud cavitation exhibits unstable transient characteristics, with constantly changing scales and oscillating boundaries. Cavities shed from the rear of the main cavitation region move towards the tip clearance of the adjacent blade, causing the tip clearance cavitation (TCC). This has a certain impact on the flow structure in the pump, leading to a decline in pump performance. Collapsed cavities on the pressure side result in blade erosion and lead to vibration and noise.

(3) As the *NPSH* decreases, the frequency of cloud cavitation shedding increases, the scale of the cavitation cloud at the leading edge of the blade decreases, and the scale of the cavitation cloud accumulated at the rear of the flow passage increases. During the critical cavitation stage, the cavitation cloud distributed at the leading edge of the blade is unable to maintain its boundary and rapidly sheds in the form of the perpendicular cavitation vortex (PCV). During the breakdown cavitation stage, a large-scale cavitation cloud forms in the flow passage, even blocking the entire flow passage, and is cut by the adjacent blade as the impeller rotates.

ACKNOWLEDGEMENTS

This work was funded by the China Postdoctoral Science Foundation Funded Project (Grant No. 2023M733355), Jiangsu University Youth Talent Development Program (2020), the Chunhui Program Cooperative Scientific Research Project of the Ministry of Education, Research Project of State Key Laboratory of Mechanical System and Vibration (Grant No. MSV202203), Natural Science Foundation of China (Grant No. 51906085, U20A20292).

Thanks to Dr. Li Yajie for improving the English writing of this paper.

CONFLICT OF INTEREST

The authors declare that there are no conflicts of interest.

AUTHORS CONTRIBUTION

Yun Long: Conceptualization, Methodology, Supervision, Visualization; **Zhen Zhou:** Data curation, Formal analysis, Writing–Original draft; **Jinqing Zhong:**

Data Curation, Validation, Writing – Original draft; **Hanqiao Han:** Supervision, Writing – review & editing.

REFERENCES

Arabnejad, M. H., Svennberg, U., & Bensow, R. E. (2021). Numerical assessment of cavitation erosion risk using incompressible simulation of cavitating flows. *Wear*, *464*, 203529. https://doi.org/10.1016/j.wear.2020.203529

Arabnejad, M. H., Svennberg, U., & Bensow, R. E. (2022). Numerical assessment of cavitation erosion risk in a commercial water-jet pump. *Journal of Fluids Engineering*, *144*(5), 051201. https://doi.org/10.1115/1.4052634

Cao, S., Goulas, A., Wu, Y., Tsukamoto, H., Peng, G., Liu, W., Zhao, L., & Cao, B. (1999, July, 18-23). *Three-dimensional turbulent flow in a centrifugal pump impeller under design and off-design operating conditions*. FEDSM-6872 Proceedings of the ASME Fluids Engineering Division.

Guedes, A., Kueny, J. L., Ciocan, G. D., & Avellan, F. (2002). *Unsteady rotor-stator analysis of hydraulic pump-turbine: CFD and experimental approach.* 21st IAHR Symposium on hydraulic machinery and systems.

Guleren, K. M., & Pinarbasi, A. (2004). Numerical simulation of the stalled flow within a vaned centrifugal pump. *Proceedings of the Institution of Mechanical Engineers, Part C: Journal of Mechanical Engineering Science*, *218*(4), 425-435. https://doi.org/10.1177/095440620421800407

Huang, R., Wang, Y., Du, T., Luo, X., Zhang, W., & Dai, Y. (2021). Mechanism analyses of the unsteady vortical cavitation behaviors for a waterjet pump in a non-uniform inflow. *Ocean Engineering*, *233*, 108798. https://doi.org/10.1016/j.oceaneng.2021.108798

Huang, S., Song, Y., Yin, J., Xu, R., & Wang, D. (2022). Research on pressure pulsation characteristics of a reactor coolant pump in hump region. *Annals of Nuclear Energy*, *178*, 109325. https://doi.org/10.1016/j.anucene.2022.109325

Iino, M., & Tanaka, K. (2004). *Numerical analysis of unstable phenomena and stabilizing modification of an impeller in a centrifugal pump*. Proceedings of 22nd IAHR symposium on hydraulic machinery and systems, Sweden, Stockholm.

Ješe, U., Fortes-Patella, R., & Dular, M. (2015, July). Numerical study of pump-turbine instabilities under pumping mode off-design conditions. In *Fluids Engineering Division Summer Meeting* (Vol. 57212, p. V001T33A018). American Society of Mechanical Engineers. https://doi.org/10.1115/AJKFluids2015-33501

Li, D. Y., Lin, S., Wang, H. J., Fu, W. W., Chen, J. X., Wei, X. Z., & Qin, D. Q. (2019). *Influence of cavitation on hump characteristics in a pump-turbine model.* IOP Conference Series: Earth and Environmental Science. IOP Publishing. https://doi.org/10.1088/1755-1315/240/7/072031

Li, D. Y., Wang, H. J., Xiang, G. M., Gong, R. Z., & Wei, X. Z. (2015, January). *Investigation on cavitation for hump characteristics of a pump turbine in pump mode.* IOP Conference Series: Materials Science and Engineering. IOP Publishing. https://doi.org/10.1088/1757-899X/72/4/042034

Li, D., Song, Y., Lin, S., Wang, H., Qin, Y., & Wei, X. (2021). Effect mechanism of cavitation on the hump characteristic of a pump-turbine. *Renewable Energy*, *167*, 369-383. https://doi.org/10.1016/j.renene.2020.11.095

Li, D., Wang, H., Qin, Y., Han, L., Wei, X., & Qin, D. (2017). Entropy production analysis of hysteresis characteristic of a pump-turbine model. *Energy Conversion and Management*, *149*, 175-191. https://doi.org/10.1016/j.enconman.2017.07.024

Li, D., Zhu, Y., Lin, S., Gong, R., Wang, H., & Luo, X. (2022). Cavitation effects on pressure fluctuation in pump-turbine hump region. *Journal of Energy Storage*, *47*, 103936. https://doi.org/10.1016/j.est.2021.103936

Li, X., Zhu, Z., Li, Y., & Chen, X. (2016). Experimental and numerical investigations of head-flow curve instability of a single-stage centrifugal pump with volute casing. *Proceedings of the Institution of Mechanical Engineers, Part A: Journal of Power and Energy*, *230*(7), 633-647. https://doi.org/10.1177/0957650916663326

Liu, D. M., Zhao, Y. Z., Liu, X. B., Ma, Y., & Wang, W. F. (2015, January). *Pump hump characteristic research based on mass transfer equation*. IOP Conference Series: Materials Science and Engineering. IOP Publishing. https://doi.org/10.1088/1757-899X/72/3/032016

Liu, Y., Wang, D., Ran, H., Xu, R., Song, Y., & Gong, B. (2021). RANS CFD analysis of hump formation mechanism in double-suction centrifugal pump under part load condition. *Energies*, *14*(20), 6815. https://doi.org/10.3390/en14206815

Long, Y., An, C., Zhu, R., & Chen, J. (2021a). Research on hydrodynamics of high velocity regions in a water-jet pump based on experimental and numerical calculations at different cavitation conditions. *Physics of Fluids*, *33*(4). https://doi.org/10.1063/5.0040618

Long, Y., Zhang, M., Zhou, Z., Zhong, J., An, C., Chen, Y., ... & Zhu, R. (2023). Research on cavitation wake vortex structures near the impeller tip of a water-jet pump. *Energies*, *16*(4), 1576. https://doi.org/10.3390/en16041576

Long, Y., Zhang, Y., Chen, J., Zhu, R., & Wang, D. (2021b). A cavitation performance prediction method for pumps: Part2-sensitivity and accuracy. *Nuclear Engineering and Technology*, *53*(11), 3612-3624. https://doi.org/10.1016/j.net.2021.05.027

Long, Y., Zhu, R., & Wang. D. (2020). A cavitation performance prediction method for pumps PART1-Proposal and feasibility. *Nuclear Engineering and Technology*, *52*(11), 2471-2478. https://doi.org/10.1016/j.net.2020.04.007

Ran, H., & Luo, X. (2018). Experimental study of instability characteristics in pump turbines. *Journal of Hydraulic Research*, *56*(6), 871-876. https://doi.org/10.1080/00221686.2017.1422193

Ran, H., Liu, Y., Luo, X., Shi, T., Xu, Y., Chen, Y., & Wang, D. (2020). Experimental comparison of two different positive slopes in one single pump turbine. *Renewable Energy*, *154*, 1218-1228. https://doi.org/10.1016/j.renene.2020.01.023

Shibata, A., Hiramatsu, H., Komaki, S., Miyagawa, K., Maeda, M., Kamei, S., Hazama, R., Sano, T., & Iino, M. (2016). Study of flow instability in off design operation of a multistage centrifugal pump. *Journal of Mechanical Science and Technology*, *30*, 493-498. https://doi.org/doi:10.1007/s12206-016-0101-1

Wang, Y., & Ding, Z. (2022). Optimization design of hump phenomenon of low specific speed centrifugal pump based on CFD and orthogonal test. *Scientific Reports*, *12*(1), 12121. https://doi.org/10.1038/s41598-022-16430-w

Xiao, Y., Yao, Y., Wang, Z., Zhang, J., Luo, Y., Zeng, C., & Zhu, W. (2016). Hydrodynamic mechanism analysis of the pump hump district for a pump-turbine. *Engineering Computations*, *33*(3). https://doi.org/10.1108/EC-02-2015-0038

Yang, J., Feng, X., Liu, X., Peng, T., Chen, Z., & Wang, Z. (2023). The suppression of hump instability inside a pump turbine in pump mode using water injection control. *Processes*, *11*(6), 1647. https://doi.org/10.3390/pr11061647

Ye, W., Ikuta, A., Chen, Y., Miyagawa, K., & Luo, X. (2020). Numerical simulation on role of the rotating stall on the hump characteristic in a mixed flow pump using modified partially averaged Navier-Stokes model. *Renewable Energy*, *166*, 91-107. https://doi.org/10.1016/j.renene.2020.11.066

Ye, W., Ikuta, A., Chen, Y., Miyagawa, K., & Luo, X. (2021). Investigation on the effect of forward skew angle blade on the hump characteristic in a mixed flow pump using modified partially averaged Navier-Stokes model. *Renewable Energy*, *170*, 118-132. https://doi.org/10.1016/j.renene.2021.01.122

Zhao, G., Liang, N., Zhang, Y., Cao, L., & Wu, D. (2021). Dynamic behaviors of blade cavitation in a water jet pump with inlet guide vanes: Effects of inflow non-uniformity and unsteadiness. *Applied Ocean Research*, *117*, 102889. https://doi.org/10.1016/j.apor.2021.102889

Zhao, H., Wang, F., Wang, C., & Wang, B. (2022). Investigation on the hump region generation mechanism of pump mode in low-head pumped hydro-storage unit. *Physics of Fluids*, *34*(11). https://doi.org/10.1063/5.0130836